How to cite: *Angew. Chem. Int. Ed.* **2021**, *60*, 2312–2321
International Edition: doi.org/10.1002/anie.202010180
German Edition: doi.org/10.1002/ange.202010180

Carbon Dioxide Activation

Selective Transformation of Nickel-Bound Formate to CO or C–C Coupling Products Triggered by Deprotonation and Steered by Alkali-Metal Ions

*Philipp Zimmermann, Deniz Ar, Marie Rößler, Patrick Holze, Beatrice Cula, Christian Herwig, and Christian Limberg**

Abstract: *The complexes $[L^{tBu}Ni(OCO\text{-}\kappa^2O,C)]M_3[N(SiMe_3)_2]_2$ (M = Li, Na, K), synthesized by deprotonation of a nickel formate complex $[L^{tBu}NiOOCH]$ with the corresponding amides $M[N(SiMe_3)_2]$, feature a Ni^{II}–CO_2^{2-} core surrounded by Lewis-acidic cations (M^+) and the influence of the latter on the behavior and reactivity was studied. The results point to a decrease of CO_2 activation within the series Li, Na, and K, which is also reflected in the reactivity with Me_3SiOTf leading to the liberation of CO and formation of a Ni–$OSiMe_3$ complex. Furthermore, in case of K^+, the $\{[K_3[N(SiMe_3)_2]_2\}^+$ shell around the Ni–CO_2^{2-} entity was shown to have a large impact on its stabilization and behavior. If the number of $K[N(SiMe_3)_2]$ equivalents used in the reaction with $[L^{tBu}NiOOCH]$ is decreased from 3 to 0.5, the deprotonated part of the precursor enters a complex reaction sequence with formation of $[L^{tBu}Ni^I(\mu\text{-}OOCH)Ni^IL^{tBu}]K$ and $[L^{tBu}Ni(C_2O_4)NiL^{tBu}]$. The same reaction at higher concentrations additionally led to the formation of a unique hexanuclear Ni^{II} complex containing both oxalate and mesoxalate ($[O_2C\text{-}CO_2\text{-}CO_2]^{4-}$) ligands.*

Introduction

Producing chemicals and fuels from ubiquitous CO_2 is a central challenge aiming at changeover towards a sustainable resource chain and much progress has been made in the last decades.[1–6] One general type of reactions that convert CO_2 is based on an initial reductive activation step, usually occurring at a metal center, to yield in M–$O(O)C^{II}H^-$, –$C^{II}(O)OH^-$, –$C^{II}O_2^{2-}$ or –$C^{III}O_2^{\bullet-}$ moieties. These species are far more reactive and can be transformed further to for example, $C^{-IV}H_4$, $H_3C^{-II}OH$, H_2C^0O or directly to $C^{II}O$ or $C^{III}{}_2O_4^{2-}$. Thus, to make headway with regard to the generation of value-added products from CO_2 mechanistic insights into the transformation of *reduced CO_2 species* are a crucial piece of information, which, however, for many systems is scarce.[7] This is, for instance, due to the fact that these intermediates are often rather elusive, so that detailed studies under controlled conditions are difficult.

Research in this direction has an impact on various different areas. As an example, in nature Ni,Fe-carbon monoxide dehydrogenases (Ni,Fe-CODHs) are catalyzing the reversible reduction of CO_2 to CO at a redox active Ni center, which is embedded in an Fe_3S_4 cluster.[8] Only recently, the intermediate resulting from the initial CO_2 contact was characterized crystallographically.[9] This revealed that the activation step is supported by a Lewis acidic Fe^{II} ion leading to a Ni-C(O)O-Fe species that features a $C^{II}O_2^{2-}$ ligand. The subsequent proceedings are still a matter of discussion. In particular it is unclear, in which step CO is liberated and what the exact role of the iron ion as a Lewis acid (LA) is. At the same time, knowledge on questions like the latter could form the basis for the rational design of artificial systems, which accomplish the LA-assisted activation of CO_2.[10–14]

In chemical laboratories a frequent and (especially in comparison with the $C^{II}O_2^{2-}$ dianion, sometimes referred to as carbonite) quite stable species formed in the reduction of CO_2 is formate. While formate as well as its corresponding acid are important chemicals and in addition have been considered as fuels,[15–17] also their further conversion and thus utilization as chemical building blocks for value-added compounds bears great potential. However, the chemistry of formate in the coordination sphere of molecular metal complexes is underdeveloped. Recently we reported on the complex $[L^{tBu}Ni(OCO\text{-}\kappa^2O,C)]Li_3[N(SiMe_3)_2]_2$, **I**, (see Scheme 1), which we synthesized from the correspondent η^2-formate precursor $[L^{tBu}NiOOCH]$, **II**, via deprotonation with $Li[N(SiMe_3)_2]$.[18] Reports on successful formate deprotonation are rather rare[12,19–21] and the synthesis of **I** has been the first example where it led to a mononuclear metal complex featuring a side-on bound CO_2^{2-} moiety; it was further shown that the same entity emerges from the activation of CO_2 at $L^{tBu}Ni^0$ units in the initial step.[18,22,23] In the present contribution we now present the results of investigations aiming at a comprehensive understanding of the properties and reactivity of the system $[L^{tBu}Ni(OCO\text{-}\kappa^2O,C)]M_3[N(SiMe_3)_2]_2$ with variation of the Lewis acidic metal ions M^+.

[*] P. Zimmermann, D. Ar, M. Rößler, Dr. P. Holze, Dr. B. Cula, Dr. C. Herwig, Prof. Dr. C. Limberg
Institut für Chemie, Humboldt-Universität zu Berlin
Brook-Taylor-Straße 2, 12489 Berlin (Germany)
E-mail: christian.limberg@chemie.hu-berlin.de
Supporting information and the ORCID identification number(s) for the author(s) of this article can be found under: https://doi.org/10.1002/anie.202010180.

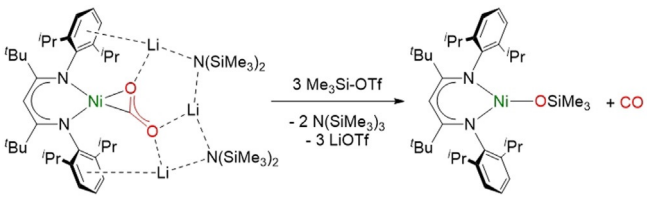

I 1

Scheme 1. Silylation of the CO_2^{2-} ligand in **I** with Me_3Si-OTf leads to the formation of complex **1** with concomitant liberation of CO.

Results and Discussion

Our studies started with gathering insights concerning the behavior of complex **I** in contact with electrophiles. **I** had proven to react with CO_2 to yield [$L^{tBu}Ni^{I}$–CO], **III**, and CO_3^{2-}.[18] Contact with a mild acid led to [$L^{tBu}Ni^{I}$–CO] (amongst others), thus resembling to some extent the conversion of CO_2^{2-} to CO in Ni,Fe-CODH,[8] however, the stoichiometry and redox chemistry in this transformation had remained unclear. Consequently, the first goal was to achieve a cleaner conversion of CO_2^{2-} to CO. To accomplish this we explored, whether—instead of providing protons in the form of acids, which partially also lead to protonation of the basic [L^{tBu}]$^-$ ligand—silylium ions can be used as proton analogues in this conversion, i.e., we studied the silylation of the CO_2^{2-} ligand in **I**.

Silylation of Ni–CO_2^{2-}—Liberation of CO

Reaction of **I** with three equivalents of TMS-OTf (Scheme 1) instantly led to [L^{tBu}NiOSiMe$_3$] (**1**), which was isolated as a microcrystalline green solid in 99% yield. A single crystal X-ray analysis revealed, that the siloxide ligand and the [L^{tBu}]$^-$ co-ligand form a Y-shaped coordination sphere for the Ni center of **1** (Figure 1).

Concomitant liberation of CO has been verified (qualitatively) via GC-MS (21% yield from headspace). Surprisingly, unlike in case of the reactions of [L^{tBu}Ni(OCO-κ^2O,C)]Li$_3$[N(SiMe$_3$)$_2$]$_2$, **I**, with H^+ (or CO_2),[18] formation of [$L^{tBu}Ni^{I}$–CO], **III**, was not observed to occur, although TMS-OTf likewise is an electrophilic reagent, that should react similarly. It thus may be inferred that **III** is formed in a secondary process, for example, through the reaction of unconsumed **I** with CO in the systems **I**/H^+ or **I**/CO_2, which is suppressed in case of TMS-OTf, as the latter reacts with **I** at sufficiently high rate (Scheme 2). Indeed, we were able to show that **I** reacts with CO to give **III** ($\nu_{CO} = 2014\ cm^{-1}$, see S6). It is thus reasonable to assume that the principal reaction of **I** with electrophiles E^+ consists of the formation of Ni-OE units with simultaneous generation of CO (Scheme 2).

Liberation of CO from Ni centers after reduction of CO_2 has been discussed quite controversially in the last years, especially with regards to the functioning of the Ni,Fe-CODH. It is still not clear, in which step of the mechanism CO is released and what the oxidation state of the Ni center is then. Scheme 3 shows two possible mechanisms, where mechanism E1 (Scheme 3, left) involves release of CO from a Ni^{II} state with subsequent reduction of Ni before CO_2 enters again and mechanism E2 (Scheme 3, right) first involves reduction to a Ni^0-CO state, followed by substitution of CO by CO_2.

In recent model studies with Ni-PNP-pincer complexes it was found that subsequent to CO_2 reduction at a Ni^0 center protonation of the resulting Ni^{II}–CO_2^{2-} complexes led to Ni^{II}–CO complexes and only after consecutive reduction to Ni^0 and addition of CO_2, CO was released (Scheme 3, middle right circle).[24,25] Recent DFT studies on the enzyme also support a mechanism where CO liberation takes place only when CO_2 enters the cycle (Scheme 3, E2), however, in this study Ni remained in the +1 oxidation state (not Ni^0) upon reduction and CO was generated from this Ni^{I}–CO state.[26] Our findings contrast the abovementioned model studies in that CO is released directly from the Ni^{II} complex (Scheme 3, middle left) and thus supports the notion that in the Ni,Fe-CODH reduction takes place after CO elimination or simultaneously. This matches the results of an X-ray diffraction analysis performed for crystals of the reduced active state of CODH grown in the absence of CO, which led to a structure that was suggested as an appropriate model for this state.[27] Obviously, the ligand environment plays a crucial role in these transformations.

Bearing in mind that not many Ni^{II}-CO complexes are known to date,[25,28–39] due to the limited ability of Ni^{II} to stabilize such entities via backbonding, we next tested whether a Ni^{II}-CO complex with the L^{tBu-} ligand system would be stable at all and reacted the cationic complex

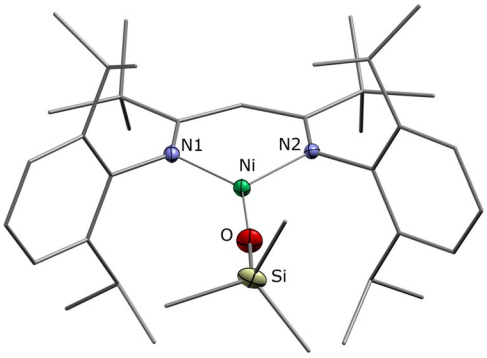

Figure 1. Molecular structure of **1**.[59] H atoms are omitted for clarity. Selected bond lengths [Å] and angles [°]: Ni-N1 1.893(1), Ni-N2 1.906(1), Ni-O 1.772(1), O-Si 1.607(2); N1-Ni-O 136.25(5), N2-Ni-O 127.20(5).

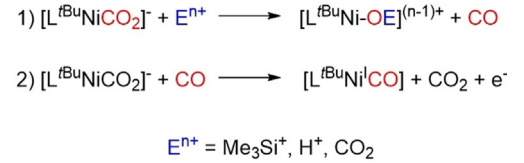

Scheme 2. 1) Formation of CO in the reaction of [$L^{tBu}NiCO_2$]$^-$ with electrophiles (E^{n+}). 2) Reaction of [$L^{tBu}NiCO_2$]$^-$ with in situ liberated CO.

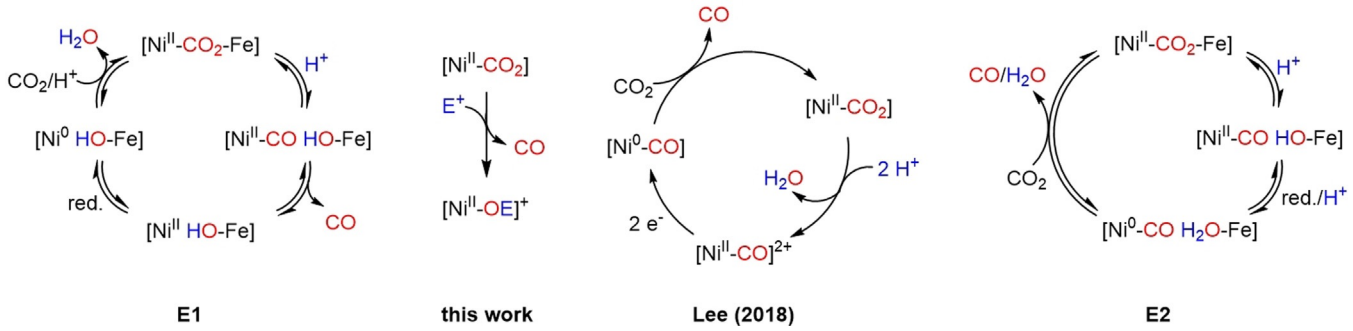

Scheme 3. Possible pathways for CO liberation in the reaction of a Ni-CO_2 complex with electrophiles E^+ (blue; for example, H^+, Me_3Si^+).

$[L^{tBu}Ni^{II}(OH_2)][B(Ar^F)_4]$ (**2**, see S3) with CO gas. A change of color from green to purple could be observed, and evaporation of all volatiles left behind a purple solid. A single-crystal X-ray analysis showed that indeed the H_2O ligand had been replaced by CO to generate $[L^{tBu}Ni^{II}(CO)][B(Ar^F)_4]$, **3**, in 82 % yield (Figure 2). The structure determination further revealed that one of the aryl rings of L^{tBu} undergoes an η^2 coordination, thus completing a square planar coordination sphere of the Ni center, which also reflects in a diamagnetic ^{1}H NMR spectrum of a solution of **3** in CD_2Cl_2.

Isolation of **3** shows that binding of CO to $L^{tBu}Ni^{II}$ is principally possible, but the initial product formed in the reaction between **I** and TMSOTf would be $L^{tBu}Ni(CO)(OSiMe_3)$, that is, a complex that can be derived from **3** by replacing the aryl donor in **3** by an anionic siloxide ligand with release of the counteranion. The failure to detect this product thus may suggest that binding of both CO and siloxide beside each other at the Ni center causes an unfavorable situation, leading to the formation of **1** with liberation of CO. To examine this hypothesis **3** was reacted with $KOSiMe_3$ in CD_2Cl_2. The color of the solution was observed to change from purple to yellow within minutes, and the ^{1}H NMR spectrum of the solution subsequently showed the complete absence of signals belonging to **3**, while new signal sets were observed that indicated the formation of a mixture of products (see S4). One of those exhibited the characteristic signal set of **1**, proving, that CO can indeed easily be replaced by $^-OSiMe_3$. Consistently, after removal of all volatiles a ν_{CO} stretching band ($[L^{tBu}Ni^{I}–CO]$) was hardly detectable in the ATR-IR spectrum of the product mixture, confirming that the reaction of **I** with TMS-OTf leads to the generation of CO as a gas. Altogether these investigations thus show, that the contact of **I** with electrophiles leads to the direct formation of CO, which is of interest also considering that the CO_2^{2-} ligand in **I** is derived from formate: Liberation of CO from HOOCH is known to occur in reactions with strong acids, however, there are only rather few examples, where formate coordinated to early transition metals (Ti,[12,20] W[21]) releases CO upon deprotonation.

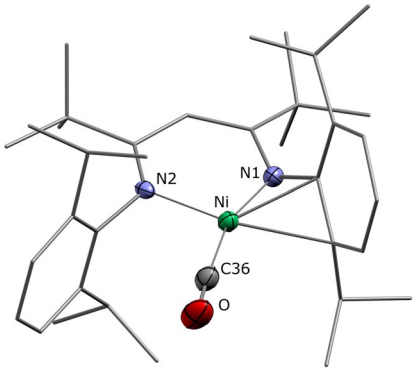

Figure 2. Molecular structure of **3**.[59] H atoms and the $[B(Ar^F)_4]^-$ counter ion are omitted for clarity. Selected bond lengths [Å] and angles [°]: Ni-N1 1.817(3), Ni-N2 1.922(3), Ni-C36 1.836(4), O-C36 1.125(5), Ni-C1 2.072(3), Ni-C2 2.230(3); N1-Ni-C36 162.1(1), N2-Ni-C36 102.2(1), Ni-C36-O 176.6(3).

As the CO_2^{2-} ligand in **I** is spanned between various metal centers (and as mentioned already can in fact also be generated by CO_2 activation[18,22,23]), we were now interested in understanding the parameters that lead to activation.

Influence of Lewis Acids on CO_2^{2-} Activation

Having learned that **I** readily generates CO in contact with electrophiles, the role of the Li_3 shell surrounding the CO_2^{2-} ligand in this conversion was explored. Initial in situ ^{1}H NMR spectroscopic studies had indicated that the synthesis of $[L^{tBu}Ni(OCO\text{-}\kappa^2O,C)]M_3[N(SiMe_3)_2]_2$ is possible also with M = Na^+ or K^+,[18] however, no structural information had been available then. We were now able to access the Na^+ derivative $[L^{tBu}Ni(OCO\text{-}\kappa^2O,C)]Na_3[N(SiMe_3)_2]_2$ (**4**) and crystallize it so that a single-crystal X-ray analysis could be performed, which revealed a structure that is similar to the one of **I** (Figure 3, left) but also shows some differences. The Ni–C bond lengths in **I** and **4** are almost identical (1.786(4) Å vs. 1.791(2) Å), but variations can be found for the different C–O bonds. While in **4** the bond of the C atom to the distal O atom is quite short (1.216(2) Å) and the one to the coordinated O atom is long (1.298(3) Å), for **I** they converge (1.234(5) Å; 1.275(5) Å). The OCO angles appear similar (127.3(2)° for **4**; 128.0(4)° for **I**).

It thus emerges that the nature of Lewis acidic centers around the CO_2^{2-} unit influences its character and it was interesting to investigate how this reflects the spectroscopic properties. Hence, first of all the ^{13}C NMR chemical shifts ($\delta^{13}C$) were compared for the Li_3, Na_3 as well as the K_3 variants. A $\delta^{13}C$ of 177.6 ppm was determined for the CO_2^{2-}

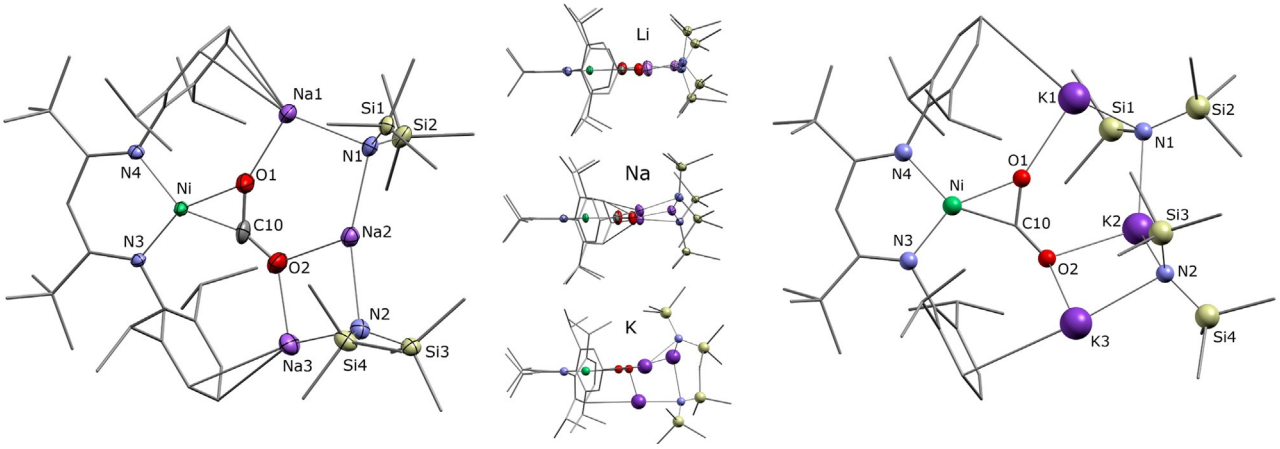

Figure 3. Left. Molecular structure of **4**·C_7H_8.[59] H atoms and co-crystallized toluene are omitted for clarity. Selected bond lengths [Å] and angles [°]: Ni-N4 1.901(2), Ni-N3 1.852(2), Ni-C10 1.791(2), Ni-O1 1.926(2), C10-O1 1.298(3), C10-O2 1.216(2); O1-C10-O2 127.3(2), Ni-C10-O2 157.5(2). Middle. Side view on Li_3, Na_3 and K_3 complexes. Right. DFT-optimized structure for the K_3 adduct. H atoms are omitted for clarity. Selected bond lengths [Å] and angles [°]: Ni-N1 1.9008, Ni-N2 1.9711, Ni-C1 1.8243, Ni-O1 2.0323, C10-O1 1.2864, C10-O2 1.2373; O1-C10-O2 129.25 Ni-C10-O2 151.21.

C atom in **I**, which shifted to 173.2 ppm upon replacement of the Li^+ ions by Na^+ ions, that is, in **4**. A further shift to 169.5 ppm is observed for the K_3-adduct. As expected, an inverse trend was found for the ν_{CO} bands in the IR spectrum of the complexes, with frequencies of 1616 cm^{-1} for Li_3, 1634 cm^{-1} for Na_3 and 1637 cm^{-1} for the K_3 adduct (1568, 1594 and 1594 cm^{-1} for the ^{13}C labelled derivatives). From these data it may be inferred that the activation of CO_2 is strongest in **I**, which is reasonable as the Li^+ ions are small and hard acids interacting strongly with the O atoms, while Na^+ and K^+ are softer and thus pull electron density to a smaller extent. Furthermore, in **4** the CO_2 appears to be somewhat more activated than in $[L^{tBu}Ni(OCO\text{-}\kappa^2O,C)]K_3[N(SiMe_3)_2]_2$ but the difference is not as pronounced as for the transition from **I** to **4**.

This raised the question in how far the differences in activation translate into the reactivity of the $NiCO_2M_3$ moieties and thus also the Na^+ and K^+ derivatives were reacted with three equivalents of TMS-OTf. Again, **1** was formed in both cases as verified by means of ^1H NMR. However, an ATR-IR spectrum of the solid crude product isolated after the reaction of the K^+ derivative revealed that, unlike in cases of the Li^+ and Na^+ derivatives, additionally $[L^{tBu}Ni^I{-}CO]$, **III**, had been formed. This implicates a slower conversion in the case of K^+ counterions, leaving enough time for the secondary process 2 as depicted in Scheme 2, that leads to **III**. While this fits to the expectations, the difference between the Na^+ and K^+ derivatives in the grade of CO_2 activation according to IR spectroscopy is not so large, that it should lead to such a sharp contrast in reactivity. Hence, steric factors had to be considered as an origin and for this purpose the structure of $[L^{tBu}Ni(OCO\text{-}\kappa^2O,C)]K_3[N(SiMe_3)_2]_2$ was calculated by DFT, using the structure of **4** as a basis for an optimization after replacement of all Na^+ ions by K^+ ions. Comparing the resulting structure to those of **I** and **4** a structural transformation becomes obvious that is most pronounced in the transition from Na^+ to K^+ (Figure 3 middle). The trend can be well illustrated, comparing the angles between the planes spanned by the $(N)_2Ni(CO_2)$ core and the plane defined by the three alkali metal cations, respectively. The small Li^+ ions integrate themselves almost perfectly into the $(N)_2Ni(CO_2)$ plane (3.0° deviation) and in fact even the amide N atoms almost lie in the same plane, too (N to plane distances 0.35 Å and 0.08 Å). For Na^+, the twist angle between the two planes rises to 8.2°, and now the N atoms deviate from the main plane by 1.10 Å and 0.28 Å. Finally, in case of the large K^+ ions the distortion becomes dramatic and the twist angle increases to 43.3°. This can clearly be seen in Figure 3, where it also becomes obvious, that in such a structure the CO_2^{2-} unit is shielded more strongly by the $SiMe_3$ groups of the $[N(SiMe_3)_2]^-$ ligands than in case of the two other derivatives, thus explaining the comparatively low reactivity.

As discussed, the contact with a Lewis acidic center can prepare a CO_2^{2-} ligand, formed via CO_2 activation at a reduced transition metal moiety, for the elimination of CO (Scheme 4). However, a $M{-}CO_2^{2-}$ moiety generated by formate deprotonation has a further option if M is redox active: an intramolecular single electron transfer leading to $CO_2^{\bullet-}$-derived products and it seems likely that this process will also be influenced by LAs. While there is no report on a system where both pathways were accessible so far, notably, this is the case in the system described here, controlled by the

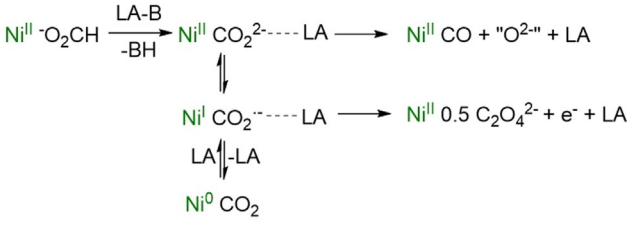

Scheme 4. Pathways for generation and reactivity of reduced CO_2 fragments with coordination of LAs.

incorporated Lewis acidic center, as will be outlined in the next paragraph.

Deprotonation with K[N(SiMe$_3$)$_2$]—Nickel Formate to Oxalate

Having shown that the nature of M^+ influences the degree of activation, we hypothesized that the number of ions M^+ will have an effect as well and started an investigation employing less than three equivalents of M[N(SiMe$_3$)$_2$]. For M = Li$^+$ or Na$^+$ this led to incomplete conversions to the corresponding CO_2 adducts **I** and **4** only. While, as described above, it is possible to also generate the K_3-analogue of **I** and **4**, namely by slow addition of [L$^{t\text{Bu}}$NiOOCH], **II**, to three equivalents of K[N(SiMe$_3$)$_2$], the deprotonation of **II** with just one equivalent of K[N(SiMe$_3$)$_2$] in C_6D_6 leads to a mixture of paramagnetic and diamagnetic products, according to a ^{1}H NMR spectrum recorded subsequently. In order to accomplish a more uniform reaction, deprotonation was carried out then with only 0.5 equivalents of K[N(SiMe$_3$)$_2$] in C_6D_6, which proved sufficient to convert all [L$^{t\text{Bu}}$NiOOCH], **II**, employed, as evidenced by the complete disappearance of all of its signals in the ^{1}H NMR spectrum. The latter revealed the concomitant formation of minor amounts of **1**, as well as the signal sets for two paramagnetic complexes that formed as the main products. One of those was identified as the known Ni oxalate complex [L$^{t\text{Bu}}$Ni(C$_2$O$_4$)NiL$^{t\text{Bu}}$], **IV**.[22] The second species shows paramagnetically broadened signals in the ^{1}H NMR spectrum, commonly observed for Ni$^{\text{I}}$ compounds and the presence of Ni$^{\text{I}}$ was indeed confirmed by EPR spectroscopy, showing a rhombic signal (best simulated for a 1:1 ratio of two very similar species, Figure 4, left). Hence, under these conditions deprotonation obviously triggers an electron transfer from the CO_2^{2-} ligand (generated by deprotonation of half of the [L$^{t\text{Bu}}$Ni$^{\text{II}}$OOCH], **II**, present) to a Ni$^{\text{II}}$ center (which presumably belongs to the second half equivalent of **II**, considering that all **II** is consumed). This would lead to a Ni$^{\text{I}}$ species and formally a $CO_2^{\bullet-}$ radical anion that likely represents the origin of the oxalate found in the second product **IV**. The electron transfer mentioned could either occur directly from a Ni$^{\text{II}}$-CO_2^{2-} unit, or, subsequent to an initial intramolecular electron transfer, from a Ni$^{\text{I}}$-$CO_2^{\bullet-}$ unit. Two equivalents of the Ni$^{\text{II}}$-$CO_2^{\bullet-}$ entities thus generated can then dimerize to give **IV**, leaving formally behind two equivalents of K[L$^{t\text{Bu}}$Ni$^{\text{I}}$OOCH], the fate of which is investigated in the following.

Electron Transfer—Nickel(I) Formate

To simulate this situation, **II**, was reacted with KC_8, which led to the formation of a vibrant red solution. Its ^{1}H NMR spectrum exhibited a set of paramagnetically broadened signals, which indeed matched the ones observed beside the signal set of **IV** after the reaction with K[N(SiMe$_3$)$_2$]. Moreover, in the EPR spectrum a rhombic signal appeared, which was very similar to one observed before (Figure 4, right). After filtration and evaporation of the volatiles [L$^{t\text{Bu}}$Ni$^{\text{I}}$(μ-OOCH)Ni$^{\text{I}}$L$^{t\text{Bu}}$]K (**5**) could be isolated as a vibrant red solid in 53 % yield. X-ray analysis of single crystals revealed a structure where two L$^{t\text{Bu}}$Ni$^{\text{I}}$ moieties are bridged by a formate ligand and a K$^+$ ion (Figure 5). Thus, the decrease of the oxidation state from +1 to +2 has led to a change of the binding mode of the formate ligand from η^2 to η^1 and thus to a change of the coordination sphere from square planar to

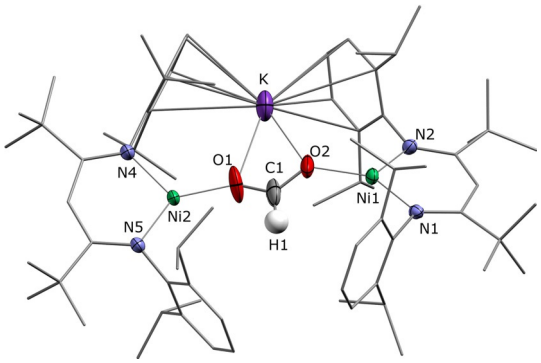

Figure 5. Molecular structure of **5**·2(Et$_2$O).[59] H atoms and Et$_2$O molecules are omitted for clarity. Selected bond lengths [Å] and angles [°]: Ni1-N1 1.861(2), Ni1-N2 1.886(2), Ni2-N5 1.866(2), Ni2-N4 1.896(2), Ni1-O2 1.894(3), Ni2-O1 1.905(3), C1-H1 1.03(3), K-O1 2.672(4), K-O2 2.681(2), C1-O1 1.245(5), C1-O2 1.237(6); O1-C1-O2 121.4(4), Ni1-C1-Ni2 169.6(2).

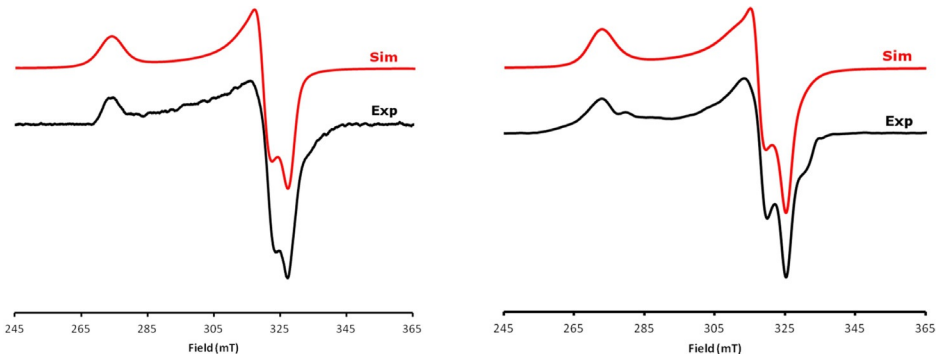

Figure 4. X-band EPR spectrum (26 K, 9.39 GHz) of the reaction mixture resulting from the reaction between **II** and 0.5 equivalents K[N(SiMe$_3$)$_2$] in C_6D_6 (black) and powder simulation for g = 2.47, 2.14, 2.07 and g = 2.48, 2.13, 2.08 (red). Right. EPR spectrum (26 K, 9.46 GHz) of **5** in C_6D_6 (black) and powder simulation for g = 2.47, 2.11, 2.09 and g = 2.46, 2.11, 2.06 (red).

trigonal planar, which is plausible. The ATR-IR spectrum of pure **5** exhibits an asymmetric CO_2 stretching vibration at 1565 cm^{-1} (Figure 6c), which shifts to 1525 cm^{-1} when the ^{13}C labelled formate precursor is utilized. This absorption band can also be found in the ATR-IR spectrum of the product mixture isolated after the reaction between [L^{tBu}NiOOCH] with 0.5 equiv. of KHMDS in C_6D_6 (Figure 6a) beside the characteristic CO stretching vibration of [L^{tBu}Ni-(C_2O_4)NiL^{tBu}], **IV** (Figure 6b). Altogether the findings lead to a stoichiometry as shown in Scheme 5 for the reaction of **II** with 0.5 equiv of K[N($SiMe_3$)$_2$].

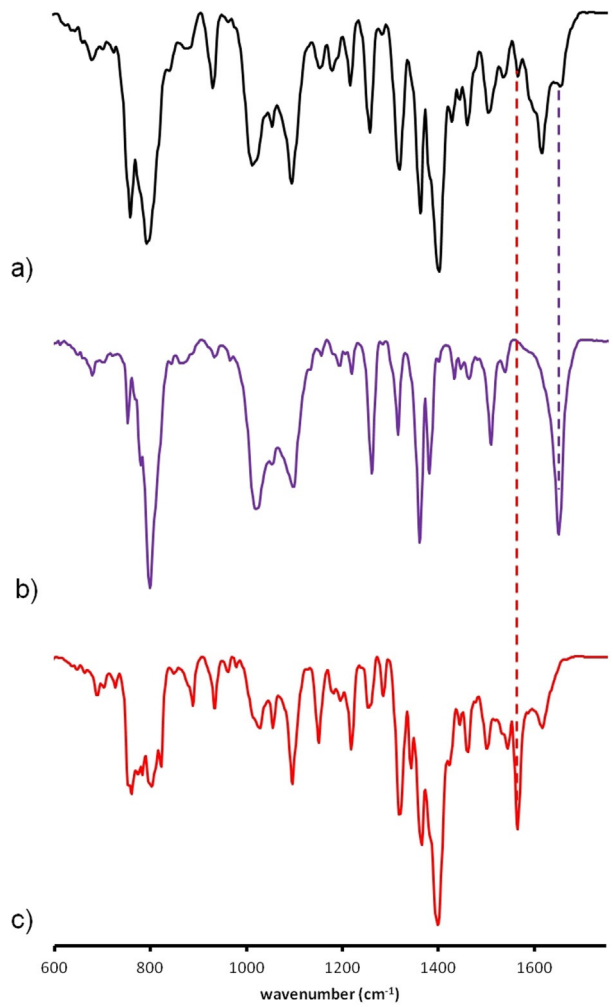

Figure 6. ATR-IR spectra of the reaction mixture resulting from the reaction between **II** and 0.5 equiv. K[N($SiMe_3$)$_2$] (a, black), pure oxalate complex **IV** (b, purple) and pure Ni^I formate complex **4** (c, red). Dotted lines indicate the correlation of the characteristic bands between a and b (1648 cm^{-1}, dotted purple line) and between a and c (1565 cm^{-1}, dotted red line).

Reaction of [$L^{tBu}Ni^I$(μ-OOCH)Ni^IL^{tBu}]K, **5**, with one equivalent of K[N($SiMe_3$)$_2$] in C_6D_6 does not lead to a significant decrease of the signals of **5** in the ^1H NMR spectrum. Accordingly, the η^2 coordination as in **II** appears to be a prerequisite for formate deprotonation. With this knowledge the reaction of **II** with more than half an equivalent of K[N($SiMe_3$)$_2$] was revisited. Small amounts of K[N($SiMe_3$)$_2$] were added stepwise to a solution of ^{13}C-labelled **II** and the proceedings monitored by means of ^1H and ^{13}C NMR spectroscopy (see S22). As outlined above, addition of 0.5 equiv. of K[N($SiMe_3$)$_2$] led to the vanishing of all characteristic signals of **II**, while the signals for oxalate complex **IV** and Ni^I formate **5** reached a maximum intensity. Adding more K[N($SiMe_3$)$_2$] led to the decrease of the signals of complex **IV** and the evolution of a new signal set that could be assigned to [L^{tBu}Ni–N($SiMe_3$)$_2$] (**6**, see S7), until one equivalent of K[N($SiMe_3$)$_2$] had been added in total. Accordingly, K[N($SiMe_3$)$_2$] preferably deprotonates **II**, forming **IV** and **5**, however, after completion of this conversion, K[N($SiMe_3$)$_2$] displaces the oxalate ligand, with concomitant precipitation of $K_2C_2O_4$. The formation of **1** as a minor side product can also be observed and may be rationalized by a minor side reaction of in situ generated **6** with traces of CO (see S8).

Intermediate of Oxalate Formation

The formation of **IV** from complex **II** is remarkable, as the direct transformation of formate to oxalate so far has only been achieved via thermal decomposition, calcination or at elevated temperatures and high pressures from bulk CO_3^{2-} (via formate intermediates) but is unknown in coordination chemistry.[40–45] There are only a few examples for oxalate formation directly from CO_2[22,46–52] and one precedent case, where the reaction of formate derived CO_2^{2-} with CO_2 led to oxalate.[19]

Thus, having clarified the stoichiometry of the reaction between [L^{tBu}NiOOCH], **II**, and K[N($SiMe_3$)$_2$], the mechanism of oxalate formation shifted into our focus. As discussed at the end of the last but one section a conceivable intermediate is, for instance, [$L^{tBu}Ni^I(OCO)^{\bullet-}$]K, **A**, namely the product of an intramolecular electron transfer within [$L^{tBu}Ni^{II}(CO_2)^{2-}$]K (see Figure 7). This does not occur within [L^{tBu}Ni(OCO-κ^2*O*,*C*)]K_3[N($SiMe_3$)$_2$]$_2$ as there two further K^+

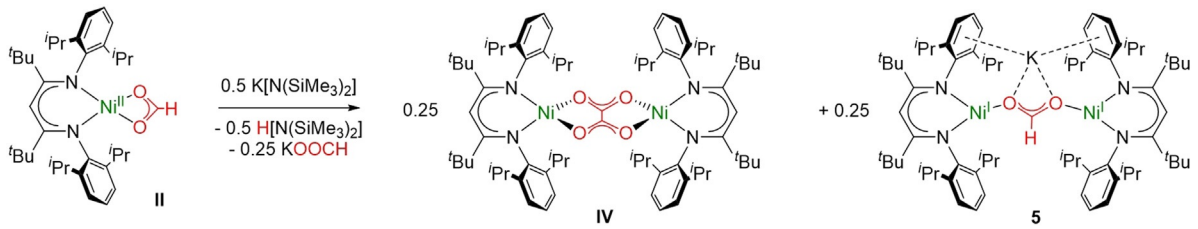

Scheme 5. Reaction scheme for the deprotonation of L^{tBu}NiOOCH with 0.5 equivalents of K[N($SiMe_3$)$_2$].

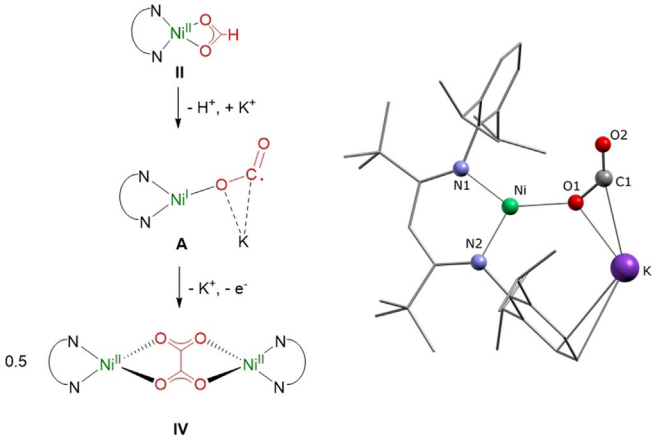

Figure 7. Left. Possible intermediate **A** leading to oxalate formation. Right. DFT-optimized structure for **A**. H atoms are omitted for clarity.

ions pull electron density. As many attempts to trap an intermediate failed, we pursued information through computational studies and modelling of the binding situation in this species. As the starting structure for a geometrical optimization of intermediate **A** we used the structural data of [$L^{tBu}Ni^{I}NCO$]K (**8**, see S9), which is isoelectronic with a $Ni^{I}(CO_2)$ complex, and exchanged the cyanate ligand by $CO_2^{\bullet-}$. The resulting structure (Figure 7, left) is stable with a Ni^{I} ion binding a bent $CO_2^{\bullet-}$ ligand (135.8°; 134° for $CO_2^{\bullet-}$[53]), supported by a K^+ ion, which interacts with the C atom and the Ni bound O atom of the $CO_2^{\bullet-}$ ligand. A very similar coordination mode with an exposed C atom has been proposed as the initial intermediate for CO_2 reduction to oxalate catalyzed by Cu complexes.[47] In the system discussed here, intermediate A would transfer an electron (and K^+) to unconsumed **II**, forming half an equivalent of **IV**.

Nickel Mesoxalate

In order to quantify the formation of the oxalate complex, crystallization attempts from benzene and hexane were conducted. In case of benzene (ca. 0.03 M) this gave solely purple crystals of the oxalate complex [$L^{tBu}Ni(C_2O_4)NiL^{tBu}$] (**IV**, 12 % absolute yield, 48 % relative yield). However, when working at high concentrations (ca. 0.15 M), from hexane solutions repeatedly and reproducibly also small orange crystals grew, that is, a further product was generated at high concentrations. Extraction with Et_2O and subsequent crystallization led to the enrichment of the orange crystals (see S10) and single-crystal X-ray crystallographic analysis revealed the structure of the unique multinuclear complex [$(L^{tBu}Ni)_6$-$(C_2O_4)_2(C_3O_6)_2K_6$] (**9**, Figure 8). The quality of the crystals did not allow an anisotropic refinement of all atoms during the solution of the structure, and hence the latter does not permit a discussion of metric parameters, but the molecular structure determined and the constitution are without doubt. **9**, which was formed in up to 9 % yield based on formate (6 % based on $L^{tBu}Ni$), contains, as **IV**, oxalate ligands, but also ligands with the configuration C_3O_6. Accordingly, three formate-derived CO_2 units have been coupled, which to our knowledge has never been reported so far. However, while the formation of oxalate ($C_2O_4^{2-}$) from two $CO_2^{\bullet-}$ species (vide supra) is straight forward, a threefold coupling would give the unknown radical $C_3O_6^{\bullet3-}$. Therefore, in a more realistic scenario two $CO_2^{\bullet-}$ equivalents and one CO_2^{2-} entity are combined yielding in the fourfold deprotonated form of dihydroxymalonic acid ($C_3O_6^{4-}$), which indeed is known as the hydrate of mesoxalic acid and represents a stable compound; for its formation routes via reaction of oxalate with CO_2^{2-} or of a $C_2O_4^{\bullet3-}$ intermediate with $CO_2^{\bullet-}$ are conceivable. **9** then contains two quadruply charged mesoxalate and two doubly negatively charged oxalate anions as well as six $[L^{tBu}]^-$ ligands. This leads to 18 negative charges which are compensated by six K^+ ions and six Ni^{II} ions, partly with tetrahedral and partly with square planar coordination

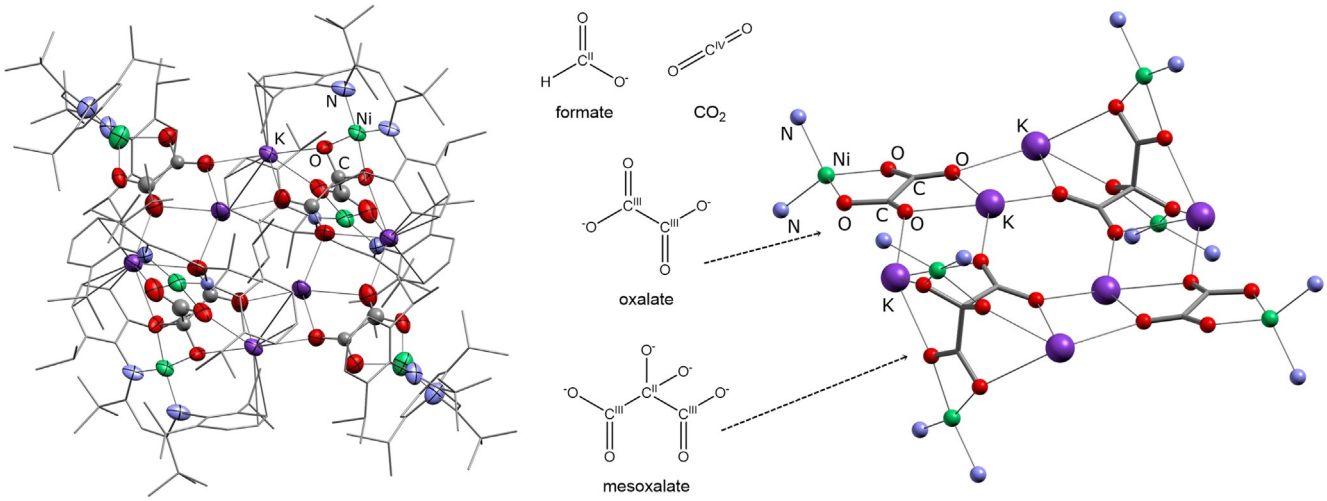

Figure 8. Left: Molecular structure of **9**·2 Et_2O.[59] Atoms that could not be refined as ellipsoids are depicted as balls. Middle. Formate and CO_2 and C–C coupling products. Right: Ball and Stick structure of the core of **9**·2 Et_2O. H atoms, Et_2O molecules and $[L^{tBu}]^-$ C atoms are omitted for clarity.

spheres, which is reasonable (note that the oxalate complex **IV** has tetrahedrally coordinated Ni centers, while **II** features a square planar coordination).

Separation of **9** from residual **IV** proved possible by extraction with MeCN that dissolves **9** to give a clear orange solution, from which an orange solid was isolated. However, storage of such solutions for crystallization leads to the precipitation of a white solid, indicating a certain instability of **IV** in MeCN. Thus, all analytical methods had to be applied within a short period of time after contact with MeCN.

The ATR-IR spectrum of **9** shows bands at 1666, 1617, 1588 and 1572 cm^{-1} in the ν_{CO} region, originating from the different carbonyl groups in the oxalate and mesoxalate ligands (1648 cm^{-1} for **IV**).

The ^1H NMR spectrum displays a combination of diamagnetic and paramagnetically shifted signal sets, as one would expect due to the different coordination environments of the six Ni centers (four square planar; two tetrahedral) in the crystal structure. While a detailed assignment of the signal sets is not possible, the ratio of the integrals from paramagnetic to diamagnetic signals should be around 1:2 or less (depending on how perfect the square planar coordination modes are maintained in solution), matching the 1:1.6 found for solutions of **IV** in [D_3]acetonitrile.

In the ^{13}C NMR spectrum of MeCN-d_3 and C_6D_6 solutions of **9** neither characteristic signals for oxalate nor for mesoxalate could be detected (the commercially available dihydroxymalonic acid disodium salt resonates at 171 and 91 ppm in D_2O), not even after ^{13}C-labelling. This is not surprising as also the corresponding ^{13}C NMR signal of the oxalate ligand in **IV** eluded detection due to its connection with the paramagnetic Ni^{II} centers. However, trying to study the in situ formation of **9** through deprotonation of ^{13C}**II** in hexane-d_{14} or C_6D_6 in an NMR tube sealed with a J. Young valve, after 4 days a characteristic set of signals at 177.7 ppm (dd, $^1J_{CC} = 57.8$ Hz) and 103.9 ppm (t, $^1J_{CC} = 57.8$ Hz) could be detected (see S10; compare: $^1J_{CC}$ of 1,2–^{13}C oxalic acid diethyl ester is 58.5 Hz). This consolidates the formation of mesoxalate, and its detection by ^{13}C NMR spectroscopy in this experiment likely became possible, as **9** is not stable in solution over four days, so that the ligands get detached from the paramagnetic Ni centers.

Mesoxalate is found rather rarely in coordination chemistry. There are reports of Pd and Cu complexes with mesoxalate ligands, generated through decomposition (after heating/time) of D-erythrulose ($C_4H_8O_4$; Pd)[54] or D-glucuronate ($C_5H_8O_6$; Cu).[55] Although it does not concern mesoxalate directly, a publication by Meyer and co-workers is noteworthy in this context, too, as it describes the reaction of CO_2 with a coordinated diketone-derived enolate (an oxalate equivalent) and based on this finding they envisioned that the coupling of three CO_2 building blocks should be possible.[56] The formation of **9**, which involves the reduced CO_2 species CO_2^{2-} is to our knowledge the first experimental example of a direct threefold coupling of CO_2 entities, illustrating the feasibility of such transformations. This may even be relevant to the prebiotic synthesis of organic compounds,[57,58] and motivates further attempts to synthesize multi-carbon compounds directly from formate or CO_2.

Conclusion

In summary, we have shown that in complexes of the type $[L^{tBu}Ni(OCO\text{-}\kappa^2O,C)]M_3[N(SiMe_3)_2]_2$ (M = Li, Na, K), formed via deprotonation of the formate complex with corresponding metal amides, the CO_2^{2-} ligand is prepared for facile CO elimination, which is triggered by a contact with electrophiles and influenced by the nature of the Lewis acidic alkali metal cations. Investigating the formate deprotonation with 0.5 equivalents of $K[N(SiMe_3)_2]$ we could demonstrate for the first time the oxidative coupling of formate on defined Ni sites. This yields not only in 0.25 equivalents of oxalate, but also in 0.5 reducing equivalents, leading to the formation of a dinuclear Ni^I formate complex, which explains why substoichiometric amounts of $K[N(SiMe_3)_2]$ proved sufficient to consume all formate precursor. A simple deprotonation reaction thus induces Ni reduction and the formation of a C–C coupling product.

Altogether, formate deprotonation can give rise to reduced CO_2 species, just as the direct reduction of CO_2 does, and can thus lead to the same products (CO, oxalate). However, the simplicity of a deprotonation reaction with solid precursors (instead of using gaseous CO_2) and the easy variation of counter ions makes this route very convenient for systematic analysis of reduced CO_2 species. Additionally, we were able to show that the same deprotonation reaction conducted at higher concentrations can even lead to mesoxalate, formed in an unprecedented, direct threefold coupling of reduced CO_2 units.

Hence, in summary, the combination of a Ni formate with an amide base that deprotonates and at the same time introduces Lewis acidic centers generates a versatile system that bears a lot of potential, aiming at the further utilization of formate or CO_2 to generate more complex organic molecules. Both can be employed to generate a CO_2^{2-} species at a metal center and the interaction with a LA can decide upon the proceedings. If they are strong the entity is stabilized but activated for CO elimination in contact with an electrophile, if it is weak, the positioning of the electrons can be shifted towards the metal (this of course depends on the properties of the metal), which opens up $CO_2^{\bullet-}$ chemistry. Here, coupling reactions have been studied but a trapping by other substrates is conceivable. Hence, the development of CO_2 reduction catalysts (or such that utilize formate) in this direction requires a fine balancing and (for a given central metal) testing of a variety of LAs.

Acknowledgements

Funded by the Deutsche Forschungsgemeinschaft (DFG, German Research Foundation) under Germany's Excellence Strategy—EXC 2008/1–390540038. Open access funding enabled and organized by Projekt DEAL.

Conflict of interest

The authors declare no conflict of interest.

Keywords: formate · Lewis acid · mesoxalate · nickel · oxalate

[1] H. Arakawa, M. Aresta, J. N. Armor, M. A. Barteau, E. J. Beckman, A. T. Bell, J. E. Bercaw, C. Creutz, E. Dinjus, D. A. Dixon, K. Domen, D. L. DuBois, J. Eckert, E. Fujita, D. H. Gibson, W. A. Goddard, D. W. Goodman, J. Keller, G. J. Kubas, H. H. Kung, J. E. Lyons, L. E. Manzer, T. J. Marks, K. Morokuma, K. M. Nicholas, R. Periana, L. Que, J. Rostrup-Nielson, W. M. H. Sachtler, L. D. Schmidt, A. Sen, G. A. Somorjai, P. C. Stair, B. R. Stults, W. Tumas, *Chem. Rev.* **2001**, *101*, 953 – 996.

[2] E. V. Kondratenko, G. Mul, J. Baltrusaitis, G. O. Larrazábal, J. Pérez-Ramírez, *Energy Environ. Sci.* **2013**, *6*, 3112 – 3135.

[3] W. Li, H. Wang, X. Jiang, J. Zhu, Z. Liu, X. Guo, C. Song, *RSC Adv.* **2018**, *8*, 7651 – 7669.

[4] F. Marques Mota, D. H. Kim, *Chem. Soc. Rev.* **2019**, *48*, 205 – 259.

[5] J. Wei, Q. Ge, R. Yao, Z. Wen, C. Fang, L. Guo, H. Xu, J. Sun, *Nat. Commun.* **2017**, *8*, 15174.

[6] L. T. Mika, E. Cséfalvay, Á. Németh, *Chem. Rev.* **2018**, *118*, 505 – 613.

[7] A. M. Appel, J. E. Bercaw, A. B. Bocarsly, H. Dobbek, D. L. DuBois, M. Dupuis, J. G. Ferry, E. Fujita, R. Hille, P. J. A. Kenis, C. A. Kerfeld, R. H. Morris, C. H. F. Peden, A. R. Portis, S. W. Ragsdale, T. B. Rauchfuss, J. N. H. Reek, L. C. Seefeldt, R. K. Thauer, G. L. Waldrop, *Chem. Rev.* **2013**, *113*, 6621 – 6658.

[8] M. Can, F. A. Armstrong, S. W. Ragsdale, *Chem. Rev.* **2014**, *114*, 4149 – 4174.

[9] J. Fesseler, J.-H. Jeoung, H. Dobbek, *Angew. Chem. Int. Ed.* **2015**, *54*, 8560 – 8564; *Angew. Chem.* **2015**, *127*, 8680 – 8684.

[10] J. E. Heimann, W. H. Bernskoetter, N. Hazari, *J. Am. Chem. Soc.* **2019**, *141*, 10520 – 10529.

[11] J. A. Buss, D. G. VanderVelde, T. Agapie, *J. Am. Chem. Soc.* **2018**, *140*, 10121 – 10125.

[12] A. Paparo, J. S. Silvia, T. P. Spaniol, J. Okuda, C. C. Cummins, *Chem. Eur. J.* **2018**, *24*, 17072 – 17079.

[13] M. R. Singh, Y. Kwon, Y. Lum, J. W. Ager, A. T. Bell, *J. Am. Chem. Soc.* **2016**, *138*, 13006 – 13012.

[14] D. Hong, T. Kawanishi, Y. Tsukakoshi, H. Kotani, T. Ishizuka, T. Kojima, *J. Am. Chem. Soc.* **2019**, *141*, 20309 – 20317.

[15] K. Sordakis, C. Tang, L. K. Vogt, H. Junge, P. J. Dyson, M. Beller, G. Laurenczy, *Chem. Rev.* **2018**, *118*, 372 – 433.

[16] A. Álvarez, A. Bansode, A. Urakawa, A. V. Bavykina, T. A. Wezendonk, M. Makkee, J. Gascon, F. Kapteijn, *Chem. Rev.* **2017**, *117*, 9804 – 9838.

[17] K. M. K. Yu, I. Curcic, J. Gabriel, S. C. E. Tsang, *ChemSusChem* **2008**, *1*, 893 – 899.

[18] P. Zimmermann, S. Hoof, B. Braun-Cula, C. Herwig, C. Limberg, *Angew. Chem. Int. Ed.* **2018**, *57*, 7230 – 7233; *Angew. Chem.* **2018**, *130*, 7349 – 7353.

[19] A. Paparo, J. S. Silvia, C. E. Kefalidis, T. P. Spaniol, L. Maron, J. Okuda, C. C. Cummins, *Angew. Chem. Int. Ed.* **2015**, *54*, 9115 – 9119; *Angew. Chem.* **2015**, *127*, 9243 – 9247.

[20] A. Mendiratta, J. S. Figueroa, C. C. Cummins, *Chem. Commun.* **2005**, 3403 – 3405.

[21] T. Schindler, A. Paparo, H. Nishiyama, T. P. Spaniol, H. Tsurugi, K. Mashima, J. Okuda, *Dalton Trans.* **2018**, *47*, 13328 – 13331.

[22] B. Horn, C. Limberg, C. Herwig, B. Braun, *Chem. Commun.* **2013**, *49*, 10923 – 10925.

[23] N. J. Hartmann, G. Wu, T. W. Hayton, *Chem. Sci.* **2018**, *9*, 6580 – 6588.

[24] C. Yoo, Y.-E. Kim, Y. Lee, *Acc. Chem. Res.* **2018**, *51*, 1144 – 1152.

[25] D. Sahoo, C. Yoo, Y. Lee, *J. Am. Chem. Soc.* **2018**, *140*, 2179 – 2185.

[26] R.-Z. Liao, P. E. M. Siegbahn, *Inorg. Chem.* **2019**, *58*, 7931 – 7938.

[27] J.-H. Jeoung, H. Dobbek, *Science* **2007**, *318*, 1461 – 1464.

[28] A. Castonguay, A. L. Beauchamp, D. Zargarian, *Inorg. Chem.* **2009**, *48*, 3177 – 3184.

[29] J. Forniés, A. Martín, L. F. Martín, B. Menjón, H. A. Kalamarides, L. F. Rhodes, C. S. Day, V. W. Day, *Chem. Eur. J.* **2002**, *8*, 4925 – 4934.

[30] M. Ito, T. Matsumoto, K. Tatsumi, *Inorg. Chem.* **2009**, *48*, 2215 – 2223.

[31] W.-F. Liaw, C.-H. Chen, C.-M. Lee, G.-H. Lee, S.-M. Peng, *J. Chem. Soc. Dalton Trans.* **2001**, 138 – 143.

[32] W.-F. Liaw, Y.-C. Horng, D.-S. Ou, C.-Y. Ching, G.-H. Lee, S.-M. Peng, *J. Am. Chem. Soc.* **1997**, *119*, 9299 – 9300.

[33] A. Miedaner, C. J. Curtis, S. A. Wander, P. A. Goodson, D. L. DuBois, *Organometallics* **1996**, *15*, 5185 – 5190.

[34] Y. Ohki, K. Yasumura, M. Ando, S. Shimokata, K. Tatsumi, *Proc. Natl. Acad. Sci. USA* **2010**, *107*, 3994 – 3997.

[35] C. G. Pierpont, R. Eisenberg, *Inorg. Chem.* **1972**, *11*, 828 – 832.

[36] C. Saint-Joly, A. Mari, A. Gleizes, M. Dartiguenave, Y. Dartiguenave, J. Galy, *Inorg. Chem.* **1980**, *19*, 2403 – 2410.

[37] F. Schneck, F. Schendzielorz, N. Hatami, M. Finger, C. Würtele, S. Schneider, *Angew. Chem. Int. Ed.* **2018**, *57*, 14482 – 14487; *Angew. Chem.* **2018**, *130*, 14690 – 14695.

[38] A. D. Wilson, K. Fraze, B. Twamley, S. M. Miller, D. L. DuBois, M. Rakowski DuBois, *J. Am. Chem. Soc.* **2008**, *130*, 1061 – 1068.

[39] C. Yoo, J. Kim, Y. Lee, *Organometallics* **2013**, *32*, 7195 – 7203.

[40] P. S. Lakkaraju, M. Askerka, H. Beyer, C. T. Ryan, T. Dobbins, C. Bennett, J. J. Kaczur, V. S. Batista, *ChemCatChem* **2016**, *8*, 3453 – 3457.

[41] M. C. Boswell, J. V. Dickson, *J. Am. Chem. Soc.* **1918**, *40*, 1779 – 1786.

[42] T. Meisel, Z. Halmos, K. Seybold, E. Pungor, *J. Therm. Anal.* **1975**, *7*, 73 – 80.

[43] A. Górski, A. D. Kraśnicka, *J. Therm. Anal.* **1987**, *32*, 1895 – 1904.

[44] A. Banerjee, M. W. Kanan, *ACS Cent. Sci.* **2018**, *4*, 606 – 613.

[45] A. Paparo, J. Okuda, *J. Organomet. Chem.* **2018**, *869*, 270 – 274.

[46] U. R. Pokharel, F. R. Fronczek, A. W. Maverick, *Nat. Commun.* **2014**, *5*, 5883.

[47] B. J. Cook, G. N. Di Francesco, K. A. Abboud, L. J. Murray, *J. Am. Chem. Soc.* **2018**, *140*, 5696 – 5700.

[48] R. Angamuthu, P. Byers, M. Lutz, A. L. Spek, E. Bouwman, *Science* **2010**, *327*, 313 – 315.

[49] M. Rudolph, S. Dautz, E.-G. Jäger, *J. Am. Chem. Soc.* **2000**, *122*, 10821 – 10830.

[50] K. Tanaka, Y. Kushi, K. Tsuge, K. Toyohara, T. Nishioka, K. Isobe, *Inorg. Chem.* **1998**, *37*, 120 – 126.

[51] J. Y. Becker, B. Vainas, R. Eger, L. Kaufman, *J. Chem. Soc. Chem. Commun.* **1985**, 1471 – 1472.

[52] Y.-T. Tseng, W.-M. Ching, W.-F. Liaw, T.-T. Lu, *Angew. Chem. Int. Ed.* **2020**, *59*, 11819 – 11823; *Angew. Chem.* **2020**, *132*, 11917 – 11921.

[53] J. Mascetti, *Carbon Dioxide as Chemical Feedstock* (Ed.: M. Aresta), Wiley-VCH, Weinheim, **2010**, pp. 55—88..

[54] T. Allscher, P. Klüfers, O. Labisch, *Carbohydr. Res.* **2007**, *342*, 1419 – 1426.

[55] M. Kato, A. K. Sah, T. Tanase, M. Mikuriya, *Inorg. Chem.* **2006**, *45*, 6646 – 6660.

[56] S. J. Zuend, O. P. Lam, F. W. Heinemann, K. Meyer, *Angew. Chem. Int. Ed.* **2011**, *50*, 10626 – 10630; *Angew. Chem.* **2011**, *123*, 10814 – 10818.

[57] A. Eschenmoser, *Tetrahedron* **2007**, *63*, 12821 – 12844.

[58] I. A. Berg, D. Kockelkorn, W. H. Ramos-Vera, R. F. Say, J. Zarzycki, M. Hügler, B. E. Alber, G. Fuchs, *Nat. Rev. Microbiol.* **2010**, *8*, 447 – 460.

[59] Deposition numbers 2013580, 2013581, 2013582, 2013583, 2013584, 2013585, 2013586, 2013587 and 2013588 contain the supplementary crystallographic data for this paper. These data are provided free of charge by the joint Cambridge Crystallographic Data Centre and Fachinformationszentrum Karlsruhe Access Structures service.

Manuscript received: July 24, 2020
Revised manuscript received: September 30, 2020
Accepted manuscript online: October 21, 2020
Version of record online: November 30, 2020

